Experimental Investigation of the Transonic Shock-Wave/Boundary-Layer Interaction over a Shock-Generation Bump

Zhengzhong Sun[1], Xin Miao, Chetan Jagadeesh

City, University of London, UK, EC1V 0HB

Abstract

A transonic shock-wave/boundary-layer interaction (T-SWBLI) established on a shock-generation bump has been investigated experimentally through particle image velocimetry and high-speed schlieren. The T-SWBLI flowfields have been examined in detail. The near-wall interaction region is visualized with high spatial resolution through schlieren and is further investigated through conditional statistical analysis. Special interests are placed on the unsteadiness associated with the shock-wave motion. The shock-wave locations are extracted to allow spectral analysis of the shock-wave oscillations. The Fourier modal analysis on the schlieren image ensemble is finally reported. The Fourier modes confirm the low-frequency unsteadiness in the shock-wave region and the interaction region. Moreover, the flow fluctuation in the rear part of the interaction region is found to extend into the medium-frequency regime.

1. INTRODUCTION

The transonic shock-wave/boundary-layer interaction (T-SWBLI) is a critical phenomenon underpins the present transonic flights. The occurrence of T-SWBLI over an airfoil causes flow separation, which inevitably induces drag and reduces flight efficiency. On the other hand, the T-SWBLI is unsteady in nature. The normal shock-wave exhibits large-scale motion across the airfoil surface, which is not desired in practice, as low-frequency fluctuating loads will be resulted. In the case of installed wing, the occurrence of T-SWBLI will produce additional unsteady moments for flight control. Study on the T-SWBLI started as early as when the 'sound barrier' was realised nearly a century ago. With the development of measurement techniques and simulation power, understanding on the T-SWBLI is being advanced continuously.

A comprehensive review on the recent T-SWBLI researches is offered by Giannelis et al. [1]. Reviewing the existing researches, the fundamental studies on the T-SWBLI mainly use two types of model: the 2D supercritical airfoil and the shock-generation bump. The OAT15A supercritical airfoil is one of the most investigated profiles. Jacquinn *et al*. [2] reported the shock buffeting phenomenon over this airfoil under Reynolds number $Re=3\times10^6$ and Mach number $Ma=0.7\sim0.75$. The characteristic shock oscillation frequency was revealed between 65~77 Hz. Recently, D'Aguanno *et al*. [3] also studied the OAT15A supercritical airfoil under similar Mach numbers but a smaller Reynolds number $Re=1.3\times10^6$. A higher shock oscillation frequency of 160Hz was reported, which can be attributed to the model with a shorter chord. The influence of Mach number and angle of attack onto the shock

---

buffeting at OAT15A airfoil is further investigated through unsteady Reynolds-averaged Naiver-Stokes simulation [4]. Shock buffeting on the other supercritical airfoils have also been examined. Hartmann et al. [5] studied the DRA-2303 supercritical airfoil through time-resolved particle image velocimetry (PIV) and assessed the influence of downstream acoustic disturbances onto the shock buffeting behaviour.

The shock-generation bump is another established model to produce the baseline T-SWBLI phenomenon. Delery [6] simulated the T-SWBLI with different strengths through 2D shock-generation bumps and measured the flow field in detail through Laser Doppler Anemometry. Bachalo & Johnson [7] generated the T-SWBLI through an axisymmetric circular-arc bump. These earlier experiments in the 1980s mainly focused on the time-averaged and turbulent characteristics in the T-SWBLI, such as the Reynolds shear stress. Following the development of simulation algorithms, LES and DNS have been applied into the analysis of baseline T-SWBLI [8, 9], giving rise to better resolved turbulent features. The unsteady shock-wave movement over the shock-generation bump has gradually received research interests. Bur et al. [10] studied the T-SWBLI with forced large-scale shock-wave oscillations at 10, 20 and 40Hz both experimentally and numerically. Sartor et al. [11] investigated the low-frequency unsteadiness in the T-SWBLI taking place close to the trailing edge of a shock-generation bump. A peak frequency of 300Hz was observed at the shock foot, while a medium-frequency centred at 4,000Hz was also detected. The latter medium-frequency was attributed to the vortical activities in the separated shear layer above the separation zone. Very recently, Della Posta et al. [12] simulated a T-SWBLI on a shock-generation bump through a Detached Eddy Simulation and confirmed the co-existence of the low-frequency and medium frequency unsteadiness.

Reviewing the above investigations reveals that the shock-generation bump allows the installation of a curved surface with relatively large chord. Hence a higher Reynolds number can be achieved in a non-industrial small-scale wind tunnel without losing the key characteristics of T-SWBLI. The present experimental study also makes use of the shock-generation bump to study the T-SWBLI. Complementary PIV and high-speed schlieren measurements are going to be performed to unveil the unsteady features of the present T-SWBLI. In the following sections, the experimental setup is introduced, which is followed by the result discussion. The instantaneous flow field is firstly reported, so that an overall understanding of the present T-SWBLI can be achieved. The large image ensemble delivered by the high-speed schlieren was made full use and the statistics of the schlieren intensity will be examined. The shock-wave spectrum is then studied by extracting the shock-wave location. Fourier modal analysis is also performed to provide further insights on the flow from the spectral point of view. Conclusions are finally drawn in the end.

2. EXPERIMENTAL SETUP

The T5 transonic wind tunnel, part of the UK National Wind Tunnel Facilities, at City, University of London is used as the flow facility. It is an intermittent induction-type wind tunnel. The high-speed flow is driven by four high-pressure ejectors located at the downstream of the test section. The total pressure and temperature are the same as the ambient parameters. The test section is 760mm long and has a square cross-section of 250mm by 250mm. In the present experiments, the slotted transonic liner is used. The inlet Mach number is maintained at 0.54 by adjusting the ejector pressure. The 2D shock-generation bump featuring a half-aerofoil follows the design of Rao [13]. The bump spans the entire tunnel width and has a chord of 315 mm. The bump maximum thickness

is 34.7 mm at 34.5% of the chord, resulting in a thickness to chord ratio of 11%. The bump model is mounted onto the bottom of test section. The chord-based Reynolds number for the experiment is thus 4.06×10^6, which is similar as those mentioned in the introduction section. A conceptual sketch of the model and test section is provided in figure 1.
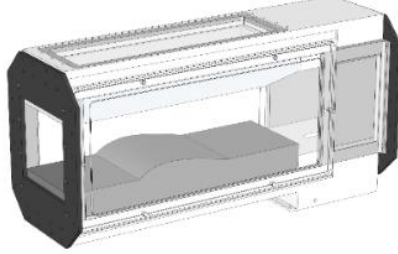

Figure 1. The wind tunnel test section and the shock-generation bump on the bottom of the test section (flow is from left to right).
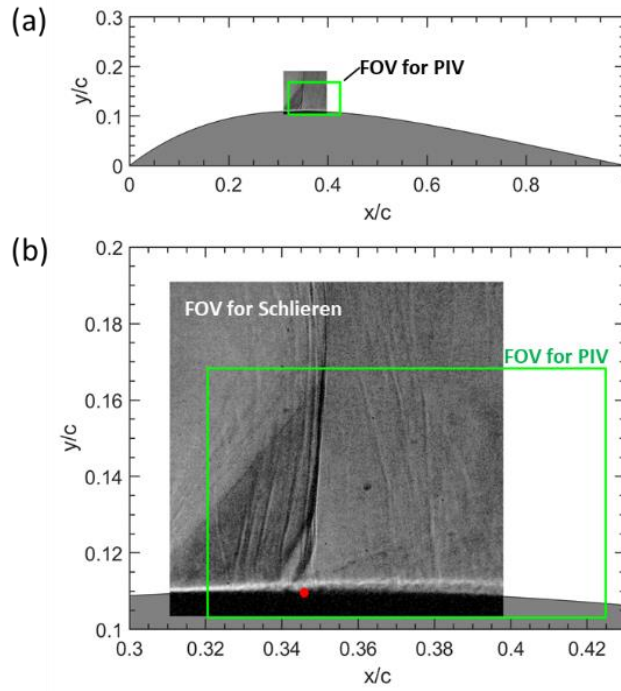

Figure 2. The Field of Views (FOVs) for schlieren and PIV over the shock-generation bump (a) and the close-up view of the two FOVs (b). The red dot indicates the apex of the bump model.

The schlieren setup has the Z-type light path. A pair of concave mirrors of 6ft focal length is used to collimate the light from a LED illuminator. The knife edge is placed horizontally to amplify the vertical density gradient, so that the turbulent boundary layer can be better visualized. A Vision Research Phantom M310 CMOS high-speed camera is used for recording. This camera allows a recording rate of 3,000fps at full frame (1080×800 pixels). In the present experiment, its sensor is cropped down to 512×512 pixels, which enables a faster recording rate of 10,000 fps. A total of 30,000 schlieren images are captured in the experiment. The schlieren Field of View (FOV) covers an area of 27.6mm×27.6mm, resulting in a spatial resolution of 0.0539 mm/pixel. The high spatial

and temporal resolutions will be made full use later to reveal the detailed flow structure as well as to analyse the shock-wave unsteadiness. The FOV of schlieren visualization with respective to the bump is shown in figure 2.

Standard planar PIV is also used to measure the velocity distribution in the present T-SWBLI. The DEHS particles of 1µm nominal diameter are generated through aerosol generator using Laskin nozzles. These particles are introduced into the settling chamber and mixed with the flow. A Litron Bernoulli dual-pulsed laser (200mJ/pulse at 532 nm) provides the flow illumination. The laser beam is delivered through an articulated arm. A light sheet of approximately 1 mm thickness is finally shaped and shot into the tunnel test section through the central open slot of the upper transonic liner. The Phantom M310 camera is used to take particle images with full resolution (1280×800 pixels). The FOV for PIV covers an area of 32.90mm×20.56mm and it is indicated by the green rectangle in figure 2. Both the laser and camera are synchronized at 15 Hz. The time separation between the two laser pulses are set to 0.6µs, resulting in a particle displacement of 5 pixels in the freestream. A total of 300 image pairs are captured. The velocity calculation is operated in the Dantec DynamicStudio 6.4 software, which includes image pre-processing (i.e. background subtraction), cross-correlation and vector conditioning. The final interrogation window is 32×16 pixels with 75% overlap. The resulted vector field therefore has horizontal spacing of 8 pixel and vertical spacing of 4 pixels. The current sub-pixel estimation procedure can faithfully reduce the measurement uncertainty below 0.1 pixel. Hence the uncertainty of the present PIV measurement is estimated to be 2% in the freestream. The parameters of the schlieren and PIV setups are summarised in Table 1.

Table 1. The parameters for schlieren and PIV.

Parameter	Schlieren	PIV
Spatial Resolution	0.0539 mm/pixel	0.0257 mm/pixel
Frame Size	512×512 pixels	1280×800 pixels
FOV	27.60×27.60 mm^2	32.90×20.56 mm^2
Frame Rate	10,000 Hz	15 Hz
Final Interrogation Window Size	-	32×16 pixels, 75% overlap
Number of Vectors	-	157×191

3. RESULTS AND DISCUSSIONS

3.1 The instantaneous flow

The instantaneous flow of the present T-SWBLI is first examined through three randomly selected schlieren snapshots shown in the top row of Figure 3, where the shock-wave is at x/c=0.335, 0.345, 0.355, respectively. Several normal shocklets are produced inside the darker region before the main shock, where the Mach number is already above 1.0. It should be mentioned that the oblique compression waves originating at around x/c=0.34 in Figure 3(b)(c) are caused by the model surface imperfection, which belongs to the trailing edge of the spanwise interchangeable slot to facilitate flow control devices. The compression wave becomes more evident when the main shock moves downstream.

The boundary-layer is visualized as the brighter strip over the bump model. The boundary-layer growth can be better appreciated through the schlieren snapshots represented by the RGB color scales, as shown in the middle row of Figure 3, where the red color corresponds to higher schlieren intensity and the blue color corresponds to lower schlieren intensity. As a result, the incoming boundary-layer is only about 0.25mm thick, but it grows to 1.13mm after interaction. The boundary-layer thickness is measured from the height of peak intensity (red in color) above the wall. Intermittent packets of high schlieren intensity can be seen at the top edge of the turbulent boundary layer after the interaction, which is associated with the vortical structures in the turbulent boundary layer.
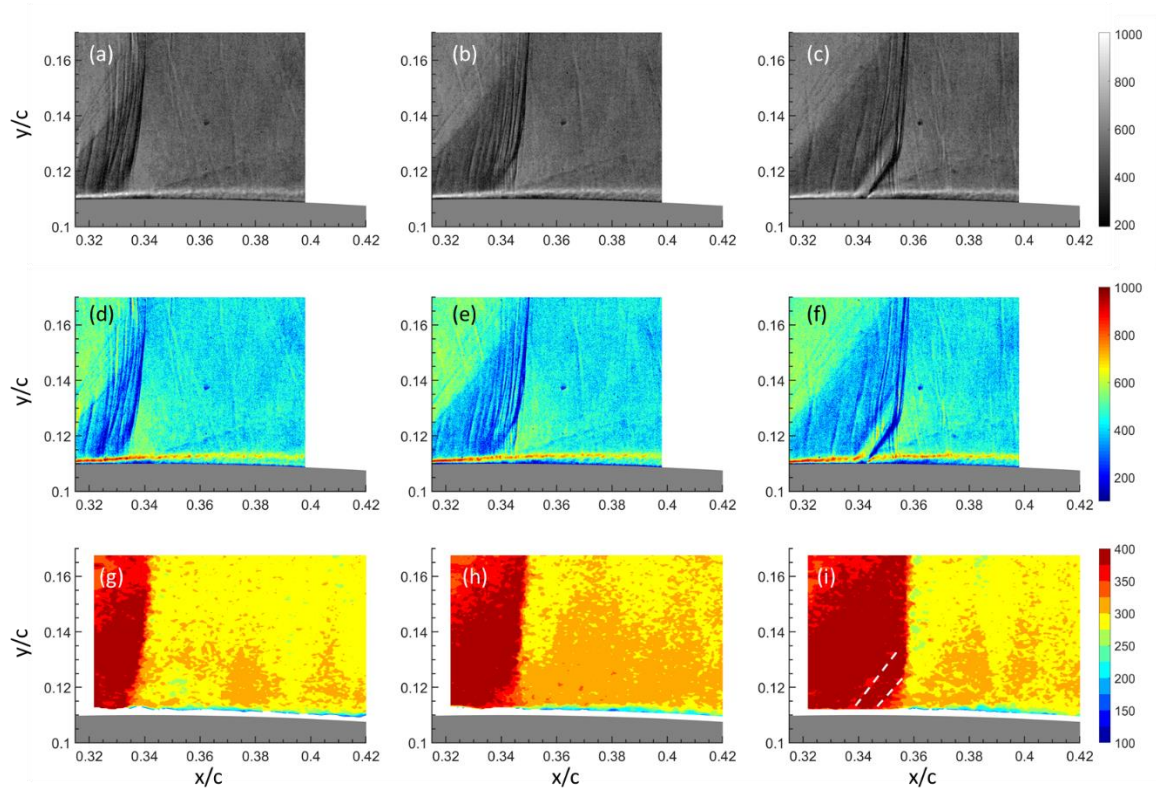

Figure 3. The instantaneous flowfield with shock-waves at x/c=0.335, 0.345, 0.355 (from left column to right column). Top row (a-c): schlieren snapshot represented by grey scale (unit: grey scale count); Middle row (d-f): schlieren snapshots represented by RGB color scale (unit: grey scale count); Bottom row (g-i): velocity field represented by streamwise velocity u (unit: m/s).

Contours of the streamwise velocity components u measured by PIV are shown in the bottom row of figure 3. These velocity contours are selected as they have similar shock-wave locations as the schlieren images. The flow upstream of the normal shock reaches a magnitude of 400 m/s, which corresponds to Ma=1.3. It decelerates abruptly to 300 m/s after the shock-wave. It should be mentioned that traces of the oblique compression waves from the surface imperfection can be seen in the velocity contours, which are indicated through the dashed line. The lower part of the flow after the shock-wave

is not completely subsonic. For example, the orange region which has velocity magnitude about 325m/s. Similar downstream supersonic region was also revealed in the T-SWBLI is the compressor cascade [14].

Because the immediate vicinity of the wall is influenced by laser reflection, the near wall region within a height of 0.63mm cannot be measured. The thin incoming boundary-layer and the interaction region are not resolved by PIV. The interaction region in the T-SWBLI in a compressor cascade was successfully visualized by Klinner et al.[14], its height was about 2mm, larger than the present T-SWBLI. The stronger interaction in [14] is due to the fact that the normal shock-wave extends the whole cascade channel and chocked the flow in the channel. Despite the near wall gap, the top part of the thickened turbulent boundary-layer can be clearly seen in figure 3, which has a velocity magnitude of about 225m/s. Moreover, it can be found that the boundary-layer thickening effect takes place right after the shock-wave.

3.2 Shock-Wave Unsteadiness

We know from the instantaneous flowfields that the shock-wave moves over the bump surface. The shock-wave location is then detected based on the schlieren intensity gradient at the height of y/c=0.136. The schlieren intensities along the entire width at y/c=0.136 in each schlieren image are extracted and synthesised together into the contour in figure 4. There is a clear interface separating the lower schlieren intensity (blue, upstream of the shock-wave) and higher schlieren intensity (green, downstream of the shock-wave). The undulating interface indicates the shock-wave movement. According to figure 4, the shock-wave oscillates within the streamwise range of x/c=0.34~0.36 at y/c=0.136, equivalent to 6.3 mm in streamwise distance.
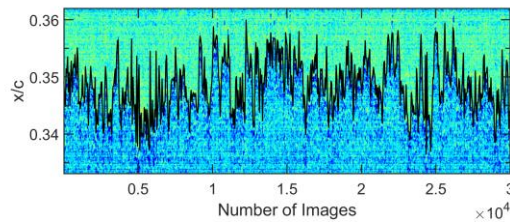

Figure 4. The synthesized schlieren intensity contour at y/c=0.136, where the two-color interface indicates the shock-wave oscillation.

Once the shock-wave location has been detected, its spectrum is processed through the Fast Fourier Transformation (FFT) with a window block containing 2048 samples and 50% overlap. The reduced FFT window delivers a smoothed spectral energy distribution at the cost of slightly coarser resolution of 4.88Hz. The pre-multiplied shock-wave spectrum is shown in figure 5. Not surprisingly, the shock oscillation exhibits intense energy within the band of 100~1,000Hz, which is consistent with the established knowledge of low-frequency unsteadiness. The peak frequency of the present T-SWBLI is

475Hz, corresponding to a Strouhal number St=0.375, where the velocity right before the shock-wave (*u*=400m/s) and the bump chord are used as the velocity and length scale, respectively. In the T-SWBLI experiment of Sartor et al. [11], the peak frequency at the shock foot was 300Hz. Della Posta et al. [12] reported a peak frequency of 221Hz at the shock foot through the simulation of a shock bump.
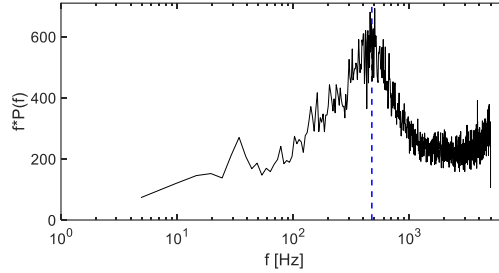

Figure 5. The pre-multiplied spectrum of shock-wave oscillation. The vertical dashed line indicates the peak frequency at 475Hz.

3.3 Conditional Statistical Analysis

Knowing the shock-wave location in the schlieren snapshot allows to conduct conditional statistical analysis of the T-SWBLI with the same shock location, which will be discussed in this sub-section. The statistics, namely the mean and Root-Mean-Square (RMS), of the schlieren intensities have recently been used to visualize the flow features that are not immediately available by observing the raw images. The RMS schlieren intensities were used by Combs *et al*. [15] to reveal the flow fluctuation in the SWBLI before a vertical cylinder. Sun *et al*. [16] further revealed the spot of peak fluctuation over the compression ramp SWBLI through the converged RMS schlieren intensities. Since the normal shock-wave in the present T-SWBLI exhibits streamwise excursion, the schlieren images with the same shock-wave location are organized to form a sub-ensemble, so that conditional statistical analysis can be performed.

The mean and RMS schlieren intensities of the T-SWBLI with shock-wave at *x/c*=0.335, 0.345 and 0.355 are examined in detail. The three sub-ensembles contain 760, 5000, 1489 images, respectively. It should be noted that a tolerance of ±2 pixels is applied for the shock-wave location to form the sub-ensemble, corresponding to a streamwise distance of ±0.108mm. Before discussing the *I_mean* and *I_rms*, their convergence is worth being checked, which is done through the evolution of their residuals with the increase of image numbers. The residuals for *I_mean* and *I_rms* follow the definitions in [16]:

$$\varepsilon_{mean}^{N} = max|I_{mean}^{N}(i,j) - I_{mean}^{N-1}(i,j)|$$

$$\varepsilon_{rms}^{N} = max|I_{rms}^{N}(i,j) - I_{rms}^{N-1}(i,j)|$$

where (i, j) is the pixel coordinate in the horizontal and vertical direction respectively, and N is the number of images used to calculate I_{mean} and I_{rms}. The evolution histories of ε_{mean} and ε_{rms} for the three sub-ensembles are shown together in figure 6. Both residual quantities reduce with the increase of image number. The ε_{rms} stays above ε_{mean}, which is understandable, as the RMS value is a second-order parameter and consequently requires a larger ensemble to converge to a similar level as that of the mean value. Among the three sub-ensembles, the one with shock-wave at x/c=0.345 contains the largest number of images, its ε_{mean} and ε_{rms} are finally below 1 count. Despite that the sub-ensemble with shock-wave at x/c=0.335 has the smallest number of images, its ε_{mean} is still below 1 count. Although its ε_{rms} converges to about 2 counts, it is found that this maximum residual belongs to the shock-wave region and is less than 1% of the peak RMS value appearing at the shock-wave location.
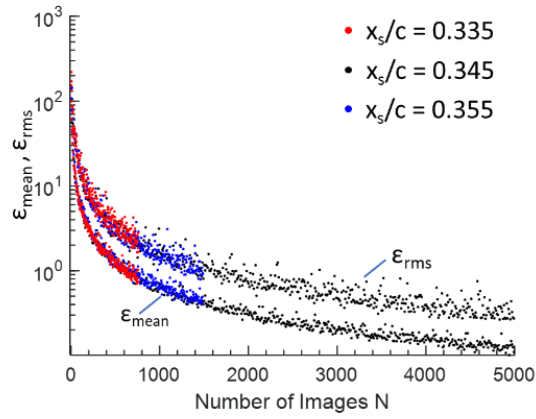

Figure 6. The residual evolutions for I_{mean} and I_{rms} in three sub-ensembles of schlieren images with shock-waves at x/c=0.335, 0.345 and 0.355.
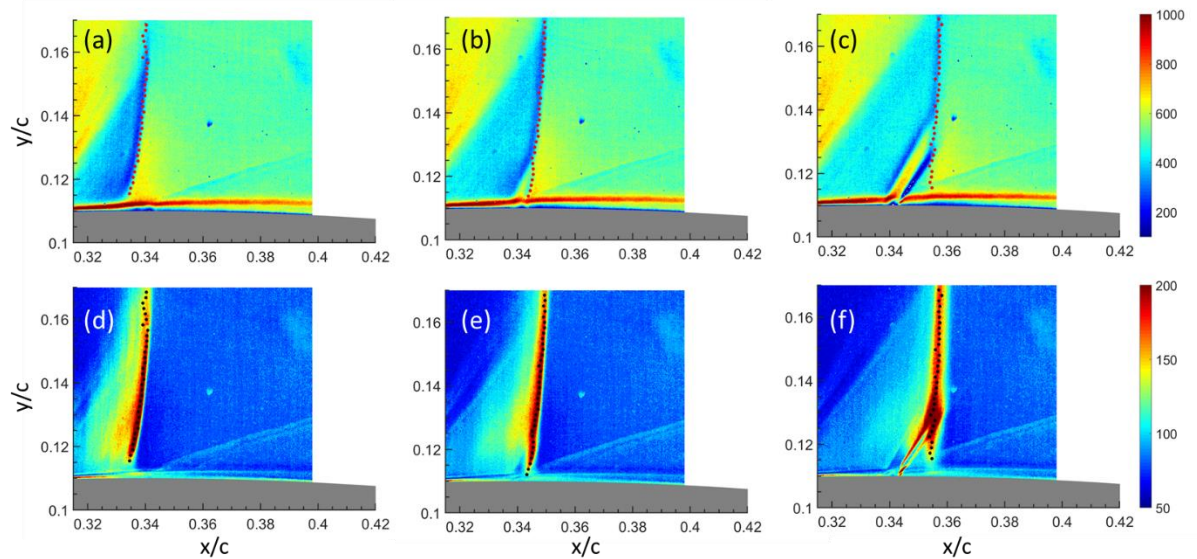

Figure 7. The mean (top row) and RMS (bottom row) schlieren images for flowfields with shock-wave at x/c=0.335. 0.345 and 0.355.

The mean and RMS schlieren intensities of the T-SWBLI with shock-wave at x/c=0.335, 0.345 and 0.355 are shown in figure 7. The mean schlieren images rendered with RGB colours (the top row of figure 7) actually offer a smoothed representation of the flow organisation. The supersonic region (blue colour) is terminated by the normal shock-wave. The shocklets before the main normal shock-wave in the instantaneous snapshots are not shown due to the averaging effect. When the main normal shock-wave moves downstream, the supersonic region becomes larger. Meanwhile, the oblique compression waves from the surface imperfection are also more evident in figure 7(b) and (c).

The I_{rms} contours are visualised in the bottom row in figure 7. The peak I_{rms} intensities are produced along the normal shock-wave. The locations of peak I_{rms} intensities are connected through the dashed lines. These lines are further overlapped onto the I_{mean} contours, and they exactly overlap with the interface where mean schlieren intensity increases sharply. The region upstream of the normal shock-wave also exhibits relatively high I_{rms} magnitude, which is contributed by the intensity fluctuation in association with the oscillating shocklets. Comparing the three I_{rms} contours finds that the high I_{rms} intensities associated with the shocklet oscillation reduces both in magnitude and in area when the main normal shock-wave is more downstream, suggesting that there are less shocklet activities in a stronger T-SWBLI.

Conditional averaging is also performed to the velocity field measured by PIV, and they are shown in figure 8. Note that conditional average is not performed for the T-SWBLI with shock-wave at x/c=0.335, because only 2 snapshots have the shock-wave close to that location. The two averaged velocity contours again confirmed that the boundary-layer thickening effect takes place right after the normal shock-wave. Abrupt velocity drop happens across the shock-wave away from the wall. The so-called 'supersonic togue' with velocity magnitude around 325 m/s happens after the shock-wave. This local supersonic region extends till x/c=0.41. The 'supersonic togue' is a typical structure in the T-SWBLI. For example, Sartor et al. [17] revealed it in the velocity contour measured by PIV.
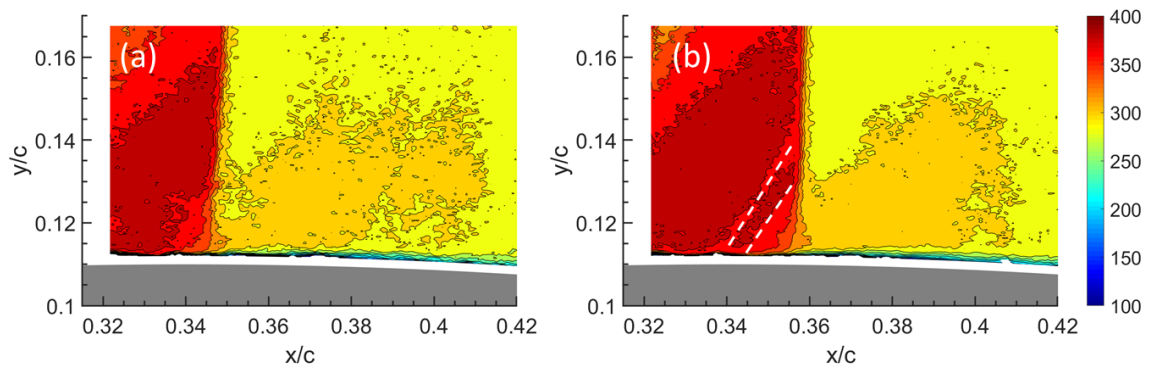

Figure 8. Conditionally averaged streamwise velocity u (unit: m/s) for flowfields with shock-waves at x/c=0.345 (a) and 0.355 (b).

The near-wall region is of great interest; Hence it is discussed with the aid of close-up views in figure 9 to figure 11. In figure 9, the distinctive stripe containing high I_{mean} intensity (red in colour) corresponds to the top edge of the turbulent boundary. It should be mentioned that the dashed lines are the connections of peak I_{mean} locations along the boundary layer. Since the surface imperfection is located at x/c=0.34, distortion can be observed in the boundary-layer due to the compression wave. We can find that a hump region of low schlieren intensity (blue color) in the immediate vicinity of the wall is produced right underneath the shock-foot. This low I_{mean} region moves downstream following the shock-wave's movement. Moreover, it extends across a longer streamwise length.
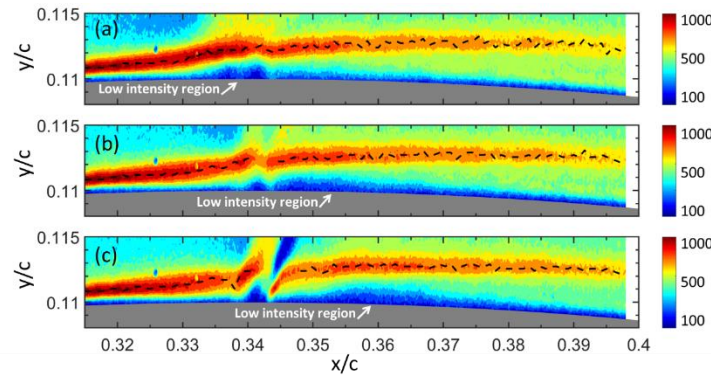

Figure 9. The near-wall region represented by the mean schlieren intensity I_{mean} with shock-wave at (a) x/c=0.335, (b) x/c=0.345 and (c) x/c=0.355.
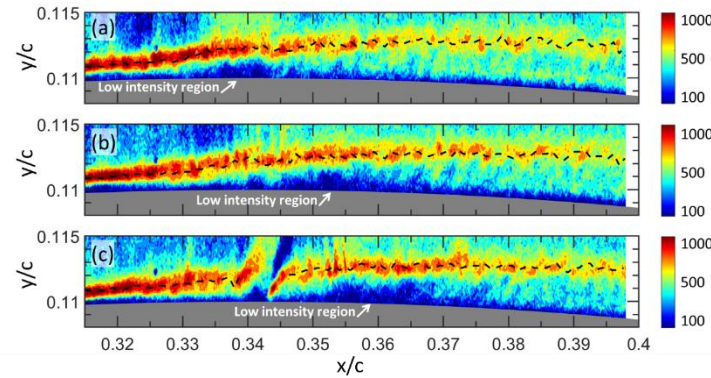

Figure 10. The near-wall region represented by the instantaneous schlieren intensity I with shock-wave at (a) x/c=0.335, (b) x/c=0.345 and (c) x/c=0.355.

The near-wall region in the instantaneous schlieren snapshots in figure 3 is also enlarged to support the discussion. Similarly, a region of low schlieren intensity is produced in each flow in figure 10 and it follows the same trend as observed in I_{mean} contour in figure 9. It is thus speculated that this region of low schlieren intensity is the interaction region where flow separation shall occur or low momentum flow is produced. A larger interaction region is resulted when the shock-wave is more downstream. The

interaction region has only a small height of 0.001c~0.002c or 0.315~0.63mm, which is missed by current PIV setup. The mean boundary layer edge is also overlapped in the instantaneous snapshot through the dashed lines. The instantaneous boundary layer clearly follows around the mean flow pattern.
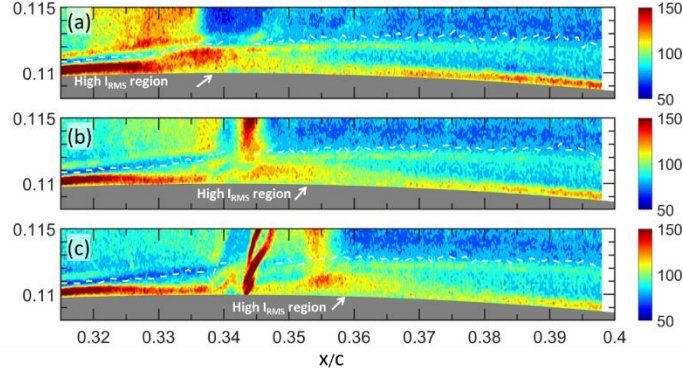

Figure 11. The near-wall region represented by the RMS schlieren intensity I$_{rms}$ with shock-wave at (a) x/c=0.335, (b) x/c=0.345 and (c) x/c=0.355.

The RMS schlieren intensity in the near-wall region, an indicator of flow fluctuation, is further displayed in figure 11, where the edge of mean boundary layer is again overlapped through the dashed lines. The high I_{rms} intensities associated with the vortical activity at the boundary layer edge is right below the mean boundary-layer edge. The interaction region of low I_{mean} magnitudes now has a high concentration of strong I_{rms} intensities, which is distinctive from the surrounding area. It thus further confirms that the interaction region in the SWBLI is characterised by flow fluctuations. Moreover, the interaction region also moves downstream with the shock-wave, which is consistent with earlier observations in the instantaneous and mean schlieren images. Closer inspection on the interaction region notices that the peak I_{rms} is slightly above the wall. It is thus conjectured as the location of separated shear layer, where both velocity and density fluctuations take place.

3.4 Fourier Model Analysis

The Fourier modes are extracted by performing FFT of the temporal variation of schlieren intensity at each pixel location within the entire ensemble. The FFT operation is based on a window block containing 2048 samples with 50% overlap, resulting in a frequency resolution of 4.88Hz. As revealed earlier in the unsteady shock-wave spectrum, the shock motion peaks at 475Hz. The Fourier mode at this peak frequency is first shown in figure 12. The shock-wave oscillation gives rise to the high spectral intensities around the mean shock locations, while the other region in the freestream has very low spectral intensity where the flow fluctuation is less severe. Due to the presence of the compression waves from wall imperfection, the high spectral intensity region associated with shock-wave is separated. Closer to the wall, there is also high spectral intensity in the interaction region, which

suggests that the flow unsteadiness inside the interaction region is locked with the shock oscillations. At this peak frequency, the interaction region extends between x/c=0.33-0.36.
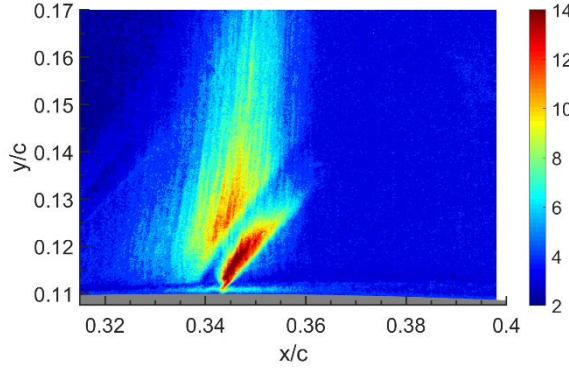

Figure 12. The schlieren Fourier mode at 475 Hz, the contour quantity has the unit of count·s.

In order to obtain an understanding of the present SWBLI in different frequency regime, the Fourier modes are averaged within three bands, namely 1~100Hz, 100~1,000Hz, 1,000~5,000Hz. Combs *et al*. [18] also used the band-averaged Fourier modes to analyse the unsteadiness in the SWBLI caused by a vertical cylinder. The present band-averaged Fourier modes are shown in figure 13. In the frequency band less than 100Hz, see figure 13(a), the dominant phenomenon is the thickening boundary layer, while the compression waves at the surface imperfection also show up. No activity associated with the normal shock-wave takes place in this frequency band, which agrees with the low-frequency unsteadiness revealed in the above sections. In the low-frequency band of 100~1,000Hz, the averaged spectral intensity distribution is similar as that at 475Hz in figure 12. In the medium-frequency band, namely 1,000~5,000Hz, the spectral intensities in the shock oscillation region is nearly halved compared to that in the low-frequency band. The interaction region still has stronger intensities than the other part of the near-wall region, suggesting that the flow fluctuation in the interaction extends to the medium-frequency regime.
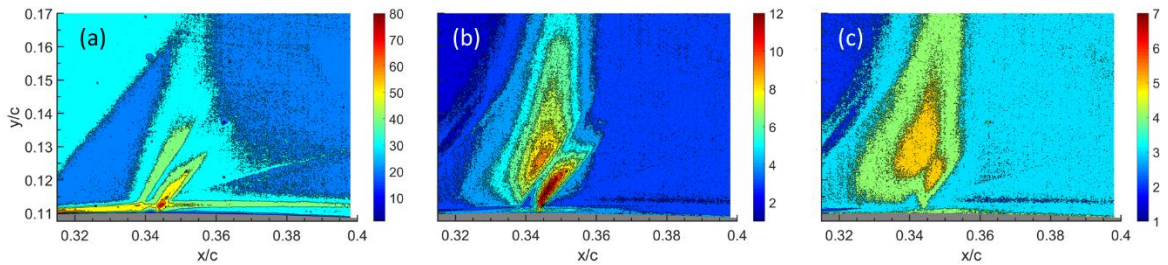

Figure 13. The band-averaged Fourier modes in the band of (a) 1~100Hz, (b) 100~1,000Hz and (c) 1,000~5,000Hz.

The near-wall region of the band-averaged Fourier modes is further investigated through the close-up views in figure 14. The very-low frequency band of 1~100Hz does not show any activity in the interaction region. Instead, the boundary layer top edge is represented through high spectral intensities,

which follows the boundary layer growth. In contrast, high spectral intensities above 5 counts·s in the interaction region can be clearly seen in the low-frequency band of 100~1,000Hz, see figure 14(b), and covers a streamwise range between $x/c = 0.335$ to 0.355. The weaker intensity of 4 counts·s (green color) extends further downstream to $x/c=0.37$. The medium-frequency regime in general exhibits lower spectral intensity in the near-wall region. The interaction region is featured by a spectral intensity of 4 counts·s. It seems that only the rear portion of the interaction region is represented, suggesting that the rear part of the unsteady interaction also has a component extending into the medium frequency domain.
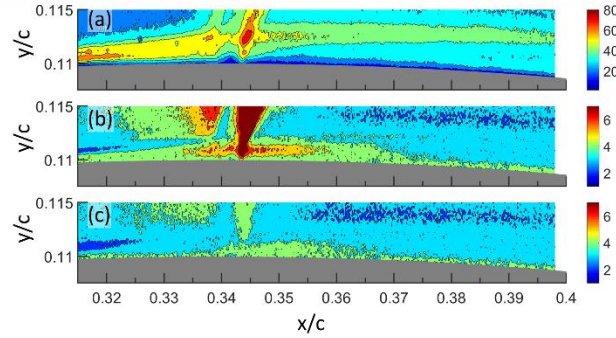

Figure 14. The close-up views of the near-wall regions in the band-averaged Fourier modes in three frequency bands: (a)1~100Hz, (b) 100~1,000Hz and (c) 1,000~5,000Hz.

The above discussions on Fourier modes have revealed that different regions in the flow field exhibit distinctive spectra. As a result, the area-averaged spectra in four specific regions, as shown in figure 15(a), are further studied. Region 1 is in the area where shock-wave oscillation takes place, hence it is selected to represent the schlieren intensity fluctuation caused by the moving shock-wave. Region 2 is in the interaction region. Region 3 and Region 4 are in the boundary layer (BL) upstream and downstream of the interaction region, respectively. The resulted area-averaged spectra are shown in figure 15(b).
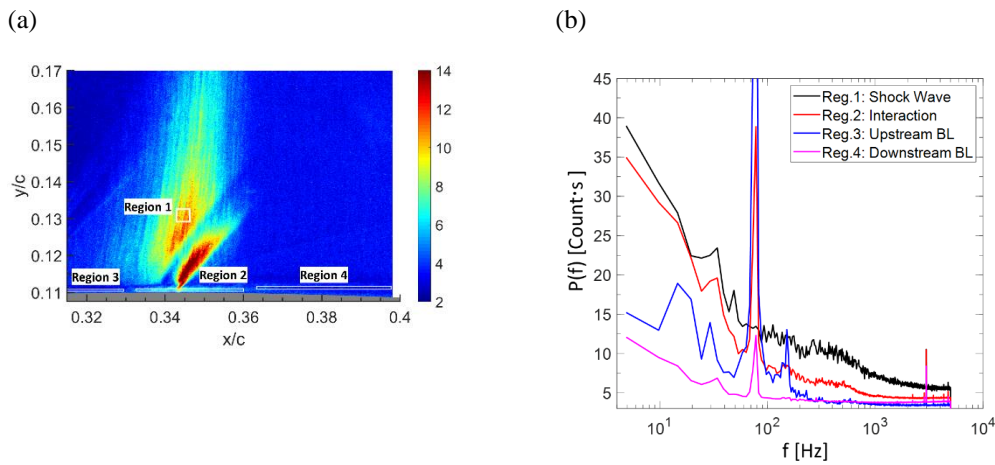

Figure 15. The area-averaged schlieren intensity spectra in four different regions: Region 1 - the shock-wave region; Region 2 – the interaction region; Region 3 – Upstream boundary-layer; Region 4 – Downstream boundary-layer.

13

The area averaged spectra are shown in figure 15(b). A spike at 78Hz occurs in the spectra in the three near-wall regions, namely region 2-4, although the intensity of spike decays from upstream region to downstream region. Note that the spike in region 2 reaches 120 counts·s and is not shown in full. This spike is likely due to the vibration of the wind tunnel model during the operation of the wind tunnel. The second harmonic of the spike at 158Hz also shows up in Region 3's spectrum. Moving to the low-frequency domain (100~1,000Hz), instead of displaying a continuous decay, a plateau of the spectra intensity is established in the shock-wave region (region 1) and the interaction region (region 2), suggesting the low-frequency unsteadiness in the SWBLI. Although region 3 exhibits some spectral intensity surrounding the second harmonic of model vibration till about 250Hz, beyond which the spectral intensity reduces to the minimal level. In the downstream region 4, no elevated intensity can be observed in the low-frequency domain. Both the shock-wave and interaction regions show up some spectral intensities in the medium-frequency domain (1,000~5,000Hz), which agrees with the observations in the band-averaged Fourier modes. However, the intensities in the mid-frequency domain in region 3 and 4 remains minimal. According to the PIV measurement, the flow velocity at the edge of the turbulent boundary layer is around 250m/s, and the boundary layer thickness varies from 1~2 mm. As a result, the characteristic frequencies in the turbulent boundary layers are estimated between 125~250kHz, which is beyond the capability of the current high-speed schlieren.

4. CONCLUSIONS

The transonic shock-wave boundary layer interactions have been investigated by high-speed schlieren and PIV. Both flow instrumentations are complementary to each other. The PIV successfully measured the velocity distribution in the T-SWBLI. The normal shock-wave was clearly shown through the abrupt velocity drop. Although the near-wall region was not fully resolved by PIV, the top edge of the turbulent boundary layer downstream of the interaction was revealed, suggesting the increase of the boundary layer thickness caused by the T-SWBLI. Both instantaneous velocity fields and the conditionally averaged ones confirmed that the thickening boundary layer is in the immediate downstream of the normal shock-wave. Moreover, the so-called 'supersonic-tongue' after the normal shock-wave and close to the wall has been revealed in the conditionally averaged velocity fields.

The present high-speed schlieren at 10kHz was demonstrated powerful in analysing the present T-SWBLI. The overall schlieren snapshots provided the shock-wave oscillation in a time-resolved manner. The shock oscillation spectrum confirmed the low-frequency unsteadiness, which peaked at 475Hz. The statistics (mean and RMS) of schlieren intensities for the sub-ensemble with the same shock-wave location were also made full use. Both the mean and RMS quantities revealed the interaction region very close to the wall, which cannot be observed in the raw instantaneous schlieren snapshots. Since the present interaction region has a height less than 1 mm, it cannot be measured by the current PIV

setup neither. Fourier modal analysis was finally performed. Both the shock-wave region and interaction region exhibited high intensity in the low-frequency domain. The rear part of the interaction region also exhibited some high spectral intensities in the medium-frequency domain.

In all, the high-speed schlieren was demonstrated a powerful tool in studying the T-SWBLIs and it is complementary to the PIV measurement. The statistics of the schlieren intensities enables flow visualizations with high spatial resolution and can resolve very close to the wall, while Fourier modal analysis provides insight from a spectral point of view.

ACKNOWLEDGEMENT

DATA AVAILABILITY STATEMENT

The data that support the findings of this study are available from the corresponding author upon reasonable request.

REFERENCES

[1] Giannelis N.F., Vio G.A., Levinski O., A review of recent developments in the understanding of transonic shock buffet, Progress in Aerospace Sciences, 2017, 92:39-84.

[2] Jacquin L., Molton P., Deck S., Maury B. & Soulevant D., Experimental study of shock oscillation over a transonic supercritical profile, AIAA J, 2009, 47(9):1985-1994.

[3] D'Aguanno A., Schrijer, F.F.J., van Oudheusden, Transonic buffet control by means of upper Gurney flaps, 54th 3AF Int. Conf. on Applied Aerodynamics, March 25-27, 2019, Paris, France.

[4] Giannelis N.F., Levinski Oleg & Vio G.A., Influence of Mach number and angle of attack on the two-dimensional transonic buffet phenomenon, Aerospace Sci. & Technology, 2018, 78:89-101.

[5] Hartmann A., Klass M. & Schroder Wolfgang, Time-resolved stereo PIV measurements of shock-boundary layer interaction on a supercritical airfoil, Exp. Fluids, 2012, 52:591-604.

[6] Delery J.M., Experimental investigation of turbulence properties in transonic shock/boundary-layer interactions, AIAA J, 1983, 21(2):180:185.

[7] Bachalo W.D. & Johnson D.A., Transonic, turbulent boundary-layer separation generated on an axisymmetric flow model, AIAA J, 1986, 24(3): 437-443.

[8] Sandham N.D., Yao Y.F., Lawal A.A., Large-eddy simulation of transonic turbulent flow over a bump, Int. J. Heat & Fluid Flow, 2003, 24:584-595.

[9] Pirozzoli S., Bernadini M & Grasso Francesco, Direct numerical simulation of transonic shock/boundary layer interaction under conditions of incipient separation, 2010, J Fluid Mech., 2010, 657:361-393.

[10] Bur R., Benay R., Galli A. & Berthouze P., Experimental and numerical study of forced shock-wave oscillations in a transonic channel, Aerospace Sci. & Technology, 2006, 10:265-278.

[11] Sartor F., Mettot C., Bur R. & Sipp D., Unsteadiness in transonic shock-wave/boundary-layer interactions: experimental investigation and global stability analysis, J. Fluid Mech., 2015, 781:550-577.

[12] Della Posta G., Martelli E., Ciottoli P.P., Stella F. & Bernardini M., Enhanced delayed DES of shock wave/boundary layer interaction in a planar transonic nozzle, Int. J. Heat and Fluid Flow, 2019, 77:359-365.

[13] Rao M.R., An experimental investigation of the use of air jet vortex generators to control shock induced boundary layer separation, 1988, Doctoral Thesis, City University London.

[14] Klinner J., Hergt A., Grund S. & Willert C.E., Experimental investigation of shock-induced separation and flow control in a transonic compressor cascade, Exp. Fluids, 2019, 60:96.

[15] Combs C.S., Schmisseur J.D., Bathel B.F. & Jones S.B., Unsteady analysis of shock-wave/boundary-layer interaction experiments at mach 4.2, 2019, AIAA J, 57(11):4715:4724.

[16] Sun Z., Gan T. & Wu Y., Shock-wave/boundary-layer interactions at compression ramps studied by high-speed schlieren, 2020, AIAA J, 58(4):1681-1688.

[17] Sartor F., Losfeld G., Bur R., PIV study on a shock-induced separation in a transonic flow, Exp Fluids, 2012, 53:815-827.

[18] Combs C.S., Lara Lash E., Kreth P.A. & Schmisseur J.D., Investigating unsteady dynamics of cylinder-induced shock-wave/transitional boundary-layer interactions, 2018. AIAA J, 56(4): 1588-1599.